Journal of The Electrochemical Society, **157** (7) C258-C267 (2010)
0013-4651/2010/157(7)/C258/10/$28.00 © The Electrochemical Society

Physicochemical Characterization of Thermally Aged Anodic Films on Magnetron-Sputtered Niobium

F. La Mantia,[a,c,*,z] M. Santamaria,[a,] F. Di Quarto,[a,**] and H. Habazaki[b,**]**

[a]*Dipartimento di Ingegneria Chimica dei Processi e dei Materiali, Università di Palermo, 90128 Palermo, Italy*
[b]*Graduate School of Engineering, Hokkaido University, Sapporo 060-8628, Japan*

The influence of thermal aging, at intermediate temperature (1 h at 250°C) and in different environments, on the electronic and solid-state properties of stabilized 160 nm thick amorphous anodic niobia, grown on magnetron-sputtered niobium metal, has been studied. A detailed physicochemical characterization of the a-Nb_2O_5/0.5 M H_2SO_4 electrolyte junction has been carried out by means of photocurrent and electrochemical impedance spectroscopy as well as by differential admittance (DA) measurements. A change in the optical bandgap (3.45 eV) of niobia film has been observed after aging (3.30 eV) at 250°C in air for 1 h. A cathodic shift (0.15–0.2 V) in the flatband potential of the junction has been observed. The frequency dependence of DA data agrees with expectations of the theory of amorphous semiconductor Schottky barrier. The fitting of both components of DA allowed to get information on the distribution of the electronic density of states as a function of energy and distance from the metal oxide interface. The DA measurements evidenced for vacuum-treated niobia film an insulating to semiconductor transition. These findings can help to explain the large changes in the measured values of capacitance, after aging, and the larger leakage current observed in niobia electrolytic capacitors.
 [DOI: 10.1149/1.3428396]

Manuscript submitted December 9, 2009; revised manuscript received April 12, 2010. Published May 25, 2010.

Anodic niobia films have been recently proposed as a possible substitute for tantala in solid-state electrolytic capacitors[1-7] or as gate oxide in organic/inorganic field effect transistors[8-11] owing to their higher dielectric constant and/or lower cost, which makes them quite attractive in low cost electronic applications. However, with respect to tantala, the electrical behavior of niobia anodic films presents some drawbacks (higher leakage current and thermal instability), which make their use rather problematic specially if employed at higher temperatures. As reported by different authors, the dielectric properties (mainly the capacitance values) of a thick anodic oxide film on niobium are greatly affected if, after formation at high potential, the oxide films are thermally aged for some hours at not too high temperature (T = 523 K) in various environments.[1,6,12]

However, niobium appears a very appealing material owing to the possibility to grow, in a large range of thicknesses and under suitable conditions, a corrosion-resistant amorphous semiconductor (a-SC) oxide film. This aspect makes anodic niobium oxide a model system for testing the validity of the theory of a-SC Schottky barriers also in semiconductor/electrolyte (SC/El) junctions.[13-17] In the more recent papers,[16-18] the theory of an amorphous SC Schottky barrier is able to explain, in a very large range of electrode potentials [high band-bending (HBB) region] and ac frequencies, both the electrochemical impedance spectroscopy (EIS) spectra and the behavior of both components of admittance as a function of the electrode potential of thin and thick films of semiconducting anodic niobia. Such investigations allowed us to overcome some of the inconsistencies (such as the frequency dependence of donor/acceptor concentration and flatband potential values) usually encountered in characterizing the electronic properties of anodic films by using the simple Mott–Schottky analysis to interpret the impedance behavior of amorphous semiconducting passive films. Moreover, from such studies we have been able to derive a more correct location of the characteristic energy levels of the SC/El junction, such as flatband potential, U_{FB}, conduction and valence band mobility edges (E_C,E_V), and some useful information on the density of electronic states (DOS) distribution in the anodic film, thus providing a deeper understanding of the solid-state properties of anodic films on metal.

In a very recent paper, a preliminary analysis of the electronic properties of aged niobia films based on EIS was carried out,[19] thus allowing us to get some information on the effect of different thermal treatments on the electrochemical behavior of anodic Nb_2O_5. In this work, a more detailed characterization of amorphous, thermally aged, anodic niobia carried out by photocurrent spectroscopy (PCS) and differential admittance (DA) measurements is reported. An interpretation of the influence of aging conditions on the solid-state and electronic properties of anodic niobia is presented based on the theory of amorphous SCs.

Experimental

Niobium films (~300 nm thick) were magnetron-sputtered onto a glass substrate using a 99.9% pure niobium target of 100 mm diameter. The deposited niobium had a body-centered cubic structure with a [110] preferred orientation.[12] These films were anodized at a constant current density of 50 A m^{-2} in 0.1 mol dm^{-3} ammonium pentaborate El at 293 K, the potential being kept constant for 1 h (called AF samples) at the final cell voltage of 50 V. Some of the anodized specimens were heat-treated in air (TA samples) or in vacuum at (0.5–1) × 10^{-5} Torr (TV samples) and 523 K for 1 h. Re-anodizing of the heat-treated specimens (TAR samples) was also carried out under the above conditions.

Impedance spectra and DA curves were recorded in 0.5 M H_2SO_4 solution by using a Parstat 2263 connected to a computer for the data acquisition. For all the experiments, a Pt net having a very high surface area was used as a counter electrode, and a saturated calomel electrode (SCE) was employed as a reference electrode. The inverse of the capacitive component of the admittance was presented in the DA plots in analogy to the classical Mott–Schottky representation and to get a rapid clue of the flatband potential value determination.

The experimental setup employed for the photoelectrochemical investigations is described elsewhere.[20] It consists of a 450 W UV/visible xenon lamp coupled with a monochromator (Kratos), which allows monochromatic irradiation of the specimen surface through the electrochemical cell quartz windows. A two-phase lock-in amplifier (EG&G) was used in connection with a mechanical chopper (frequency: 13 Hz) to separate the photocurrent from the total current circulating in the cell due to the potentiostatic control. Photocurrent spectra reported below were corrected for the relative photon efficiency of the light source at each wavelength, so that the photocurrent yield in arbitrary current units was represented in the Y axis.

* Electrochemical Society Student Member.
** Electrochemical Society Active Member.
[c] Present address: Department of Materials Science and Engineering, Stanford University, Stanford, California 94305.
[z] E-mail: lamantia@stanford.edu

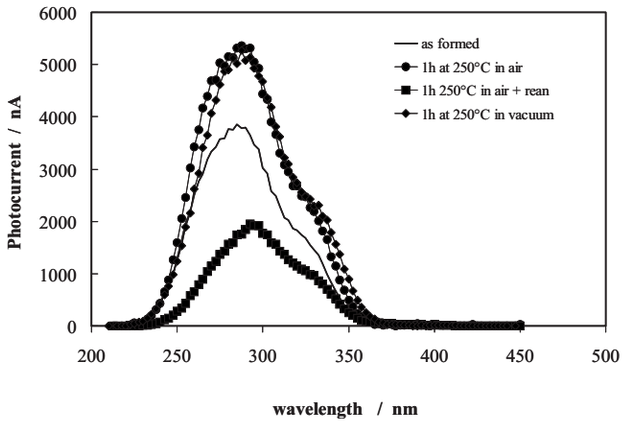

Figure 1. Raw photocurrent spectra relating to 50 V anodic films on Nb before and after different treatments, recorded in 0.5 M H_2SO_4 by polarizing the electrodes at 1 V(SCE).

Results and Discussion

Photoelectrochemical study.— In Fig. 1, we report the photocurrent spectra relating to the 50 V anodic film on Nb before and after different treatments, recorded by polarizing the electrode at 1 V(SCE) in 0.5 M H_2SO_4. In the vicinity of the bandgap, by assuming indirect (nondirect for amorphous materials[21]) optical transitions, the following equation holds[22]

$$(I_{ph}h\nu)^{0.5} \propto (h\nu - E_g) \quad [1]$$

where I_{ph} is the measured photocurrent corrected for the relative photon efficiency (photocurrent yield) of the light source at each wavelength and E_g is the mobility gap of the oxide for amorphous materials. Such a relationship assumes a direct proportionality between the photocurrent yield and the light absorption coefficient, and it holds also for thin and thick amorphous oxide films.[20,23] Equation 1 allows us to estimate the mobility gap ($E_g \approx 3.45$ eV) of the investigated films by extrapolating the $(I_{ph}h\nu)^{0.5}$ vs $h\nu$ plot to zero (see Fig. 2). Photocurrent is present at energy lower than the estimated bandgap value (see Fig. 2a), originating another linear region in the $(I_{ph}h\nu)^{0.5}$ vs $h\nu$ plot ending at around 2.95 eV, which can be associated with optical transitions involving localized states inside the mobility gap of the oxide.[21] In the presence of a DOS distribution varying linearly with energy close to the bandedges, Eq. 1 keeps holding, provided that E_g represents now the difference in energy between the conduction band mobility edge and the highest energy level of valence band localized states or the difference in energy between the valence band mobility edge and the lowest energy level of conduction band localized states.[21] Similar results have been reported for thick a-Nb_2O_5 anodic film grown on bulk metal so that this feature appears as intrinsic to anodic niobia regardless of the initial metal surface preparation.[23]

By comparing the photocurrent spectra recorded for all the investigated samples, the following aspects arise:

1. The mobility gap of anodic Nb_2O_5 is slightly reduced to 3.30 eV by the thermal treatment in air, while it is not appreciably influenced by thermal treatment in vacuum (see Table I).
2. The photocurrent tail at energy lower than the mobility gap is reduced after thermal treatment in air but not after thermal treatment in vacuum (see Fig. 2b and d).
3. The effect of thermal treatment, under air exposure, on the mobility gap value is canceled by the re-anodizing process when almost the same value of 3.44 eV is measured for the mobility gap but without tailing.

According to this, we can conclude that the thermal treatment in air

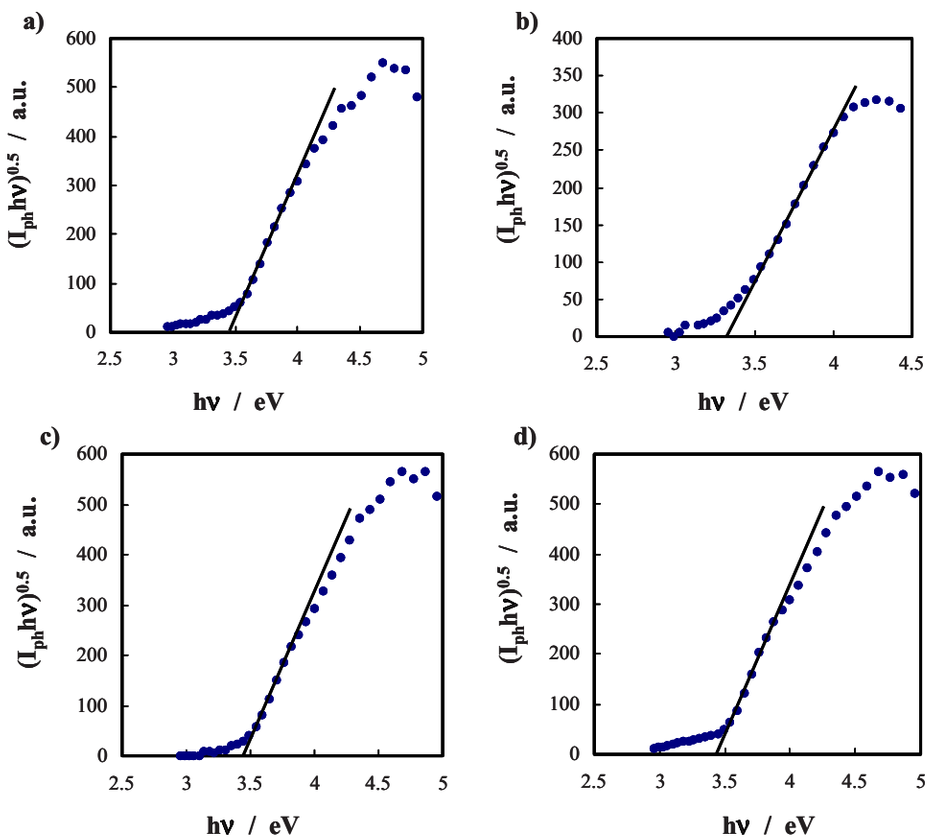

Figure 2. (Color online) $(I_{ph}h\nu)^{0.5}$ vs $h\nu$ plot relating to 50 V anodic films on Nb before and after different treatments, recorded by polarizing the electrodes at 8 V(SCE) in 0.5 M H_2SO_4.

Table I. Parameters obtained from the analysis of photocurrent spectra (Fig. 2) and photocharacteristic at λ = 320 nm (Fig. 3) according to Eq. 1 and 2, respectively (see text).

Sample	E_g (eV)	V^* [V(SCE)]	n
AF	3.45	−0.21	0.91
TA	3.30	−0.37	0.875
TAR	3.44	−0.14	0.915
TV	3.45	−0.41	0.84

is very effective in suppressing the tailing in the photocurrent spectra of niobia also after re-anodizing, probably by reducing the intensity of optical transitions between extended and localized electronic states (see below). Photocurrent vs electrode potential (photocharacteristics) curves at a constant irradiating wavelength (with $h\nu > E_g$) were recorded for all the investigated oxides by scanning the electrode potential in the cathodic direction at 10 mV s^{-1} (see Fig. 3). The I_{ph} vs U_E curves were fitted according to a power law

$$(I_{ph})^n \propto (U_E - V^*) \quad [2]$$

The best-fitting exponent, n, and the extrapolated zero photocurrent potential, V^*, which can be assumed as a rough estimate of the flatband potential, U_{FB}, are reported in Table I for a fixed wavelength (λ = 320 nm) and a constant photon flux. As expected, V^* depends on the postanodizing treatment, with the most cathodic values pertaining to niobium oxide after thermal treatment in vacuum ($V^* = -0.41$ V/SCE) or in air ($V^* = -0.37$ V/SCE). Both these values are appreciably more cathodic than the values measured for as-formed ($V^* \geq -0.21$ V/SCE) and re-anodized samples ($V^* = -0.14$ V/SCE).

As a general rule, we have to say that the V^* parameter, derived from fitting with a power law of the I_{ph} vs U_E plots, tends to assume, like the onset photocurrent potential, more anodic values with respect to the true flatband potential,[11] and the values change appreciably with a small change in n. For these reasons, whenever possible, a determination of the flatband potential in dark conditions is desirable (see DA measurements below). Moreover, in a previous work on anodic niobia,[23] thick anodic niobia film displayed V^* values anodically shifting with the intensity of illumination. However, owing to the use of the same wavelength and photon flux for all investigated samples, we can reasonably assume that the relative shift in the V^* value for the different samples, as a function of the postanodizing treatment, is a real experimental finding and not an artifact of the illumination intensity. It follows that the cathodic shift of V^* (and possibly of U_{FB}), after thermal treatment in air or under vacuum, agrees with previous observations reporting an increasing nonstoichiometry of the film after thermal treatment owing to an increased concentration of undervalent niobium into the oxide due to oxygen dissolution into the metal at the metal–oxide interface.[1,3,24] However, while the annealing in vacuum does not change the mobility gap value as well as the photocurrent tailing at lower energies, in annealing in oxygen atmosphere, we observe the disappearance of the tailing as well as a reduction of the mobility gap, E_{mg}, which decreases of ~0.10 to 0.15 eV. The reduction in E_{mg} could be related to a partial reorganization of the amorphous structure favored by a high temperature in the presence of oxygen atmosphere. This would suggest a reorganization of the oxygen ions around the Nb^{5+} ions with an increase in the short-range order and a consequent decrease in the disorder contribution to the measured optical bandgap.[20] This suggestion should agree also with the effect of the re-anodizing, which brings the optical bandgap to the original values of 3.40–3.45 eV by introducing again an increasing lattice disorder as a result of the new ion displacements under anodizing electric field.

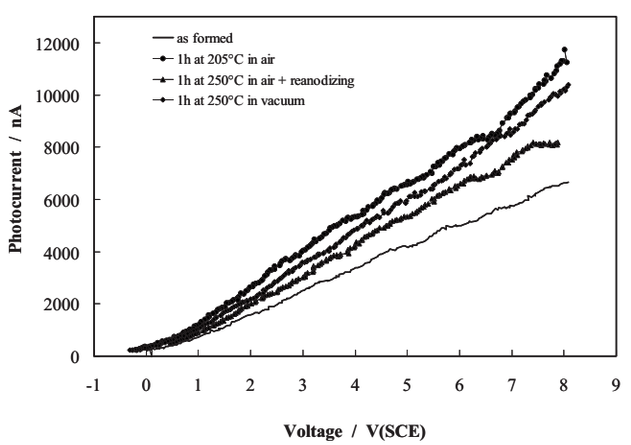

Figure 3. Photocurrent vs electrode potential curves relating to 50 V anodic films on Nb before and after different treatments, recorded at 320 nm in 0.5 M H_2SO_4 by scanning the electrode potential in the cathodic direction at 10 mV s^{-1}.

The re-anodizing process affects the optical properties of air-treated samples by increasing the optical bandgap but by keeping negligible the intensity of optical transitions involving localized states within the mobility edges, as evidenced by the lack of any appreciable tailing in the optical gap of air-treated samples after re-anodizing (Fig. 2c). These findings suggest that after air-treatment a permanent decrease in the localized DOS value occurs, while the Fermi level changes as a function of the Nb/O stoichiometric ratio. The thermal treatments favor an increase in this metal/oxygen ratio and an upraising (more cathodic V^*) of the Fermi level, while the re-anodizing processes decrease it by lowering the Fermi level (more anodic V^*) of the junction. The presence or absence of a tailing in the optical spectra depends on the localized DOS at energies below the two mobility edges, as suggested by the fact that the light absorption coefficient for a given wavelength is related to the optical transitions involving the joint initial and final DOS.[25] The presence of tailing for the AF sample as well as for the TV-treated sample must be traced, however, to different origins, and we come back on these aspects after discussing the DOS distribution, within the mobility gap of samples, derived from the DA studies.

Concerning the best-fit exponent of the photocharacteristics, for the investigated films the photocharacteristics displayed a quasi-linear (AF and TAR samples) or a slightly supralinear (TA and TV samples) behavior at longer wavelengths (λ ≥ 320 nm). Like for crystalline films, a quasi-linear or a sublinear dependence of the measured photocurrent on the applied potential is expected also for amorphous materials in the absence of trapping phenomena and for slightly absorbed light ($ad_{ox} \ll 1$). The supralinear behavior can be attributed to the presence of surface recombination phenomena (at low potential) involving the photogenerated carriers as well as to geminate recombination effects generally occurring in any material where the photogenerated carriers display very low mobility (like in amorphous materials). In the presence of geminate recombination effects, an influence of the electric field and photon energy, through the thermalization distance r_0 of the photocarriers,[20] is expected on the efficiency of photocarrier generation, which could explain the supralinear behavior of the photocharacteristics at higher band bending when the surface recombination process goes to zero. The influence of trapping of photocarriers and the geminate recombination effects on the photoelectrochemical behavior of amorphous oxide have been deeply discussed for anodic niobia[23] and other oxides in previous works where interested readers can find more details.[20]

As for the influence of postanodizing treatment on the intensity of photocurrent at constant potential, the results in Fig. 1 show that at low potentials the niobia samples, after thermal treatment in air or under vacuum, display almost the same intensity of photocurrent at any wavelength with I_{ph} values larger than those recorded on as-

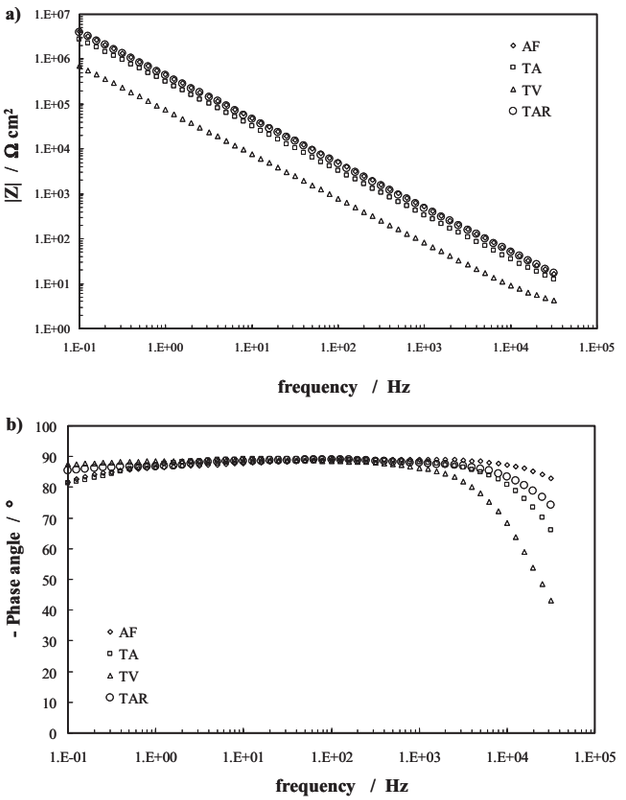

Figure 4. Bode representation of the impedance data acquired at 0.75 V(SCE) in 0.5 M H_2SO_4, relating to 50 V anodic films on Nb before and after different treatments. (a) Impedance magnitude and (b) phase angle.

formed or re-anodized samples. The beneficial effect of the thermal treatment in increasing the measured photocurrent of an illuminated anodic passive film is quite common, and it could be attributed to an improvement of the migration term in the space-charge region of the amorphous SC, owing to an increase in the photocarrier drift length[20,23] as a consequence of changes in the localized electronic DOS distribution near the band mobility edges of the oxide. However, at low electrode potential values (low electric fields into the SC) the recombination of photogenerated carriers can occur both in the space-charge region of a-Nb_2O_5 as well as at the oxide/El interface. Both these recombination processes are favored in as-formed as well as in re-anodized samples (see Fig. 1), the latter displaying the lowest external photocurrent yield at low potential. By assuming for as-formed and re-anodized samples the formation of insulating-like anodic niobia film[19] (see also admittance measurements), the lower electric field and drift mobility conspire in decreasing the drift length and then the photocurrent answer of these samples at low electrode potentials.

EIS study.— EIS spectra were recorded in 0.5 M H_2SO_4 for all the investigated samples in a wide range of electrode potentials (−0.25 to 6.0 V/SCE). The impedance spectra were analyzed using the Kramers–Kronig transforms, as explained elsewhere;[26,27] they obey the causality, linearity, and stability principles.

In Fig. 4, the Bode plot at 0.75 V(SCE) in 0.5 M H_2SO_4 is represented for all the samples. The phase shift (Fig. 4b) shows that the behavior of the Nb_2O_5 electrodes is capacitive, regardless of the thermal treatment. The differences among the samples in the high frequency region (above 1 kHz) are due to the electrolyte resistance, which changed slightly with the geometrical position of electrodes, while in the low frequency region (below 10 Hz), the different behaviors can be truly attributed to the different electronic properties.

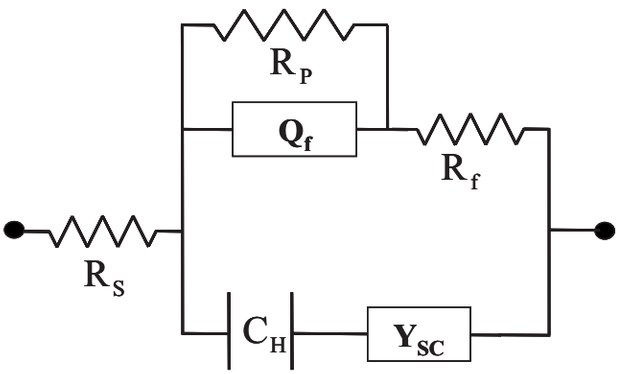

Figure 5. Equivalent electrical circuit employed to simulate the impedance of the metal/oxide/El interface (adapted from Ref. 19).

Concerning $|Z|$ (Fig. 4a), the as-formed oxide shows the highest values of impedance magnitude, which is slightly reduced by the thermal treatment in air, this last effect being canceled by the re-anodizing process. The lowest $|Z|$ is observed for the vacuum-treated sample, whose impedance is also clearly dependent on the applied potential, as discussed below. According to the transmission electron micrograph (TEM) of ultramicrotomed sections as well as to the glow discharge optical emission spectrometer analysis of the investigated films,[1] changes in the oxide film thickness with the thermal treatment are negligible so that the decrease in the modulus of the impedance for vacuum-treated samples is directly related to the change in the electronic properties of the film due to the thermal treatment.

As for the fitting of the EIS spectra, an electrical equivalent circuit quite similar to that previously used for thick anodic films[17,19] on electropolished Nb metal has been used, as reported in Fig. 5, where an arm in parallel with an ideal SC/El interface is present to take into account a possible electron-transfer reaction from/to solution (through localized surface states or directly) to/from a SC electrode conduction band.[28-30] In Table II, we reported the fitting parameters and the standard deviation obtained for the vacuum-treated sample. $R_S = 2.83\ \Omega\ cm^2$, $C_H = 2 \times 10^{-5}$ F cm^{-2}, and $n_f = 0.8$ for all the exploited electrode potential ranges (see above). From the data reported in Table II, it comes out that the arm in parallel to Y_{SC} in Fig. 5, containing the elements Q_f, R_f, and R_p, is practically negligible at any frequency and all potentials but the lowest.[19] According to these findings, the same

Table II. Fitting parameters and standard deviation obtained from the fitting of EIS spectra for the vacuum-treated sample using the equivalent circuit reported in Fig. 5. R_S = 2.83 Ω cm², C_H = 20 μF cm⁻², and n_f = 0.8 for all the polarization potentials (adapted from Ref. 19).

U_E vs SCE (V)	R_f (Ω cm²)	Q_f (μS sn cm⁻²)	R_p (MΩ cm²)	χ^2
−0.25	1.64	7.26	1.01	5.05×10^{-4}
0	1.72×10^3	4.71×10^{-1}	11.4	2.18×10^{-4}
0.25	1.35×10^6	8.99×10^{-2}	15.6	2.85×10^{-4}
0.5	6.23×10^6	6.02×10^{-2}	34.8	3.06×10^{-4}
0.75	7.73×10^6	6.09×10^{-2}	42.5	3.65×10^{-4}
1	8.85×10^6	5.90×10^{-2}	48.1	3.03×10^{-4}
1.5	8.15×10^6	5.01×10^{-2}	45.3	2.71×10^{-4}
2	7.10×10^6	4.86×10^{-2}	49.5	3.35×10^{-4}
4	5.46×10^6	4.33×10^{-2}	54.2	3.71×10^{-4}
6	3.74×10^6	4.10×10^{-2}	59.5	1.60×10^{-4}

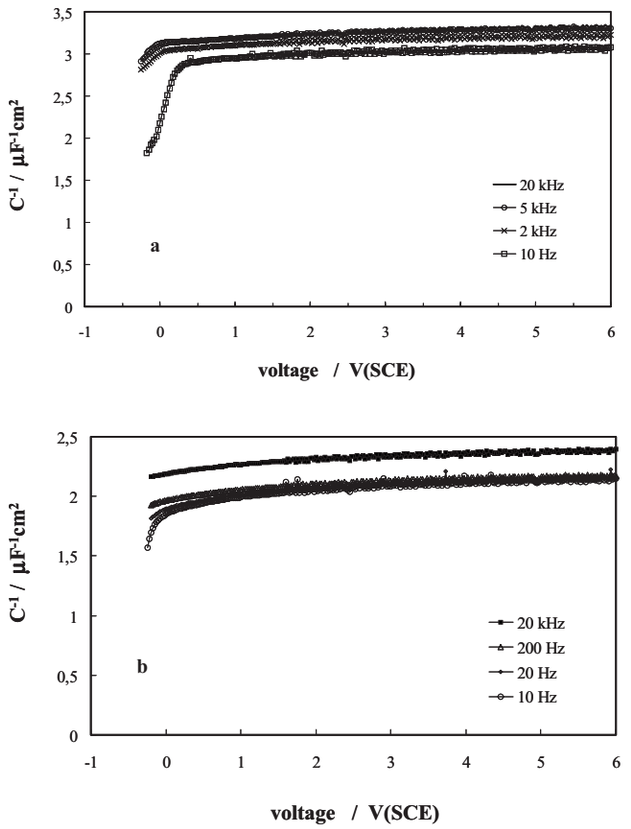

Figure 6. Inverse of differential capacitance vs U_E plots at different frequencies for (a) re-anodized air-treated niobia and (b) air-treated niobia at different frequencies. The data plotted in figure have been corrected for the equivalent series resistance and the Helmholtz double-layer capacitance (20 µF cm^{-2}).

electrical equivalent circuit has been adopted by neglecting the parallel arm to fit the DA data in the investigated frequency range (see below).

DA study.— In previous papers (Ref. 13-18 and references therein), a detailed study of the electronic properties of amorphous passive films has been carried out on the basis of the theory of the a-SC Schottky barrier, as developed in Ref. 31-35. These studies have shown that such an approach is able to provide a deeper insight on the electrical behavior and solid-state properties of passive films.

Although all films investigated in this work are amorphous,[1,12] the as-formed as well as the re-anodized samples displayed very different electrical behaviors with respect to the vacuum- and air-treated samples. Thus, we present separately the results of the DA measurements of the two groups of samples, but we discuss together, in a following section, the electronic properties of all samples.

As-formed and air-treated re-anodized samples.— As evidenced in Ref. 19, the differential capacitance of as-formed as well as of re-anodized samples is almost potential independent at different frequencies but slightly dependent on the ac frequency up to 5 kHz when the measured capacitance saturated to an almost constant value (Fig. 6a). A closer inspection of the curves for the TAR sample at lower frequencies ($f < 100$ Hz in Fig. 6a) shows a marked increase in the measured differential capacitance at the lowest electrode potentials, very close to the zero photocurrent potential V^*, which agrees with the suggestion that such a parameter is a proxy of the flatband potential of the oxide/El junction. The flattening of differential capacitance at higher frequencies as well as the trend toward a common potential-independent capacitance value agree with the expected behavior of a-SC thin films.[14,36] In fact, the width of the space-charge region in a-SC is $X_{SC} = \varepsilon\varepsilon_0/C_{SC}(\omega,\psi_S)$, and its value, both potential and frequency dependent as the capacitance of a-SC, extends across all the films with increasing ac frequency (see also the theory below). Such findings have been reported for different passive films on valve metals (Ref. 20 and references therein) including cast Nb.[14,16,17]

As for the capacitance data of as-formed and re-anodized air-treated samples, at frequencies <5 kHz, the capacitance is higher than the value expected for an ideal insulating film (see the value at $f \geq 5$ kHz) owing to a possible contribution coming from surface-state capacitance (C_{SS}) or to a width of the space-charge region lower than the whole film thickness. Because both hypotheses appeared, in principle, a plausible test of surface-state contribution to oxide capacitance was carried out by determining which value of C_{SS} to subtract to the measured capacitance at each frequency to get a value equal to that measured at the highest frequency (20 kHz). It came out that in a range of frequencies going from 10 Hz to 2 kHz, the contribution of C_{SS} varies from ~35 to ~15 nF cm^{-2} (see Fig. 6a). Such a small change in C_{SS} values does not seem compatible with the strong frequency dependence theoretically expected in such a large range of frequencies, but it appears compatible with a frequency dependence mechanism of hopping conduction in amorphous materials.[21] According to this, we are forced to conclude that the small change in capacitance value with frequency in re-anodized or as-formed samples must be attributed to the amorphous nature of the films, which agrees with the theoretically expected frequency dependence of the space-charge region width in the amorphous SC Schottky barrier[13,14,31-34] and to the microscopic mechanism of electrical conduction in the amorphous material.[21]

From the capacitance value, measured at the highest frequency (10–20 kHz), a value of relative dielectric constant in the range 53–56 was estimated for both samples of anodic niobia by using the formula for the parallel plate capacitor ($\varepsilon_{ox} = C_{ox}d_{ox}/\varepsilon_0$) and the value of film thickness measured by TEM analysis of ultramicrotomed sections (157–159 nm, according to Ref. 37). This ε_{ox} value is quite larger than that measured during the growth (ε_{ox} = 42–44) under a high electric field,[2,14,38] and the difference in ε_{ox} has been attributed to the presence of the large electrostrictive effect, as reported in Ref. 39.

According to Ord et al.,[39] the dependence of the dielectric constant from the electric field, F_{el}, can be written as

$$\varepsilon(F_{el}) = \varepsilon(0)(1 - \gamma F_{el}) \quad [3]$$

from which an average value for the parameter γ_{av} = 6.62 Å V^{-1} has been derived by using a value of electric field during the growth equal to 3.77 × 10^6 V cm^{-1} and an $\varepsilon(F_{el})$ value of 42–44 during the growth. This γ_{av} value is intermediate between those reported by Ord et al. (8.61 A/V),[39] based on ellipsometric studies, and the average value of 4.5 Å V^{-1} estimated by us on the basis of capacitance measurements at low electric field (open-circuit potential) and at the anodizing electric field. By assuming a permittivity value at zero electric field $\varepsilon(0) = 53$, the following expression has been derived for the permittivity at any other electric field F_{av}

$$\varepsilon(F) = 53(1 - 0.24 \times F_{av}/F_{an}) \quad [4]$$

where F_{av} and F_{an} represent the average and anodizing electric fields within the oxide film, respectively. In the fitting procedure of admittance curves, when a field-dependent dielectric constant was employed, the F_{av}/F_{an} ratio was approximated by the $(U_E - U_{FB})/(V_f - V_{eq})$ ratio. In this last ratio, at constant film thickness as during the DA measurements, the term at the numerator is a proxy of the average electric field into the a-SC at the U_E electrode potential, while the term in the denominator is a measure of the electric field during the growth. For stabilized films, the V_f value is equal to the film thickness multiplied for the anodizing electric field reported above, while the V_{eq} is the equilibrium potential of the reaction

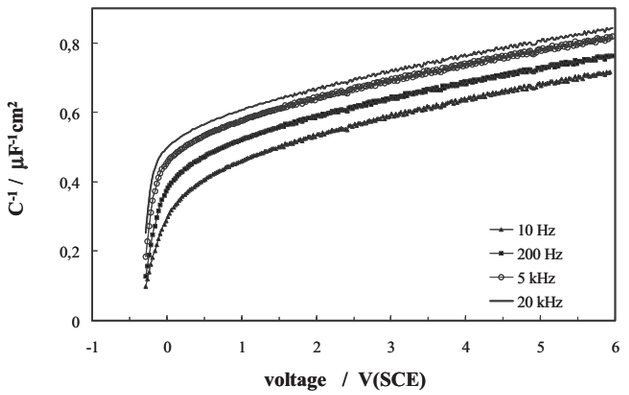

Figure 7. Inverse of differential capacitance vs U_E plots of the vacuum-treated (TV) sample at different frequencies. The data plotted in figure have been corrected for the equivalent series resistance and the Helmholtz double-layer capacitance (20 μF cm^{-2}).

$$Nb_2O_5 + 10H^+ + 10e^- = 2Nb + 5H_2O \qquad [5]$$

Vacuum- and air-treated samples.— As for the differential capacitance behavior of the TA sample, at various frequencies, it appears to agree with the amorphous nature of the oxides, as evidenced by the influence of the frequency on the differential capacitance values of the junction (see Fig. 6b). As for the differential capacitance at 20 kHz, it appears very weakly dependent on the electrode potential like for the insulating material when the space-charge region extends across the entire film. However, from the capacitance value, measured at the highest potential and by using the formula for a parallel plate capacitor ($d_{ox} = C_{ox}/\varepsilon_{ox}\varepsilon_0$) and a value of relative dielectric constant in the range 53–56, the estimated space-charge region is still appreciably less (about 70%) than the value of film thickness measured by TEM (~160 nm). At variance with the TV sample for which the theory of the a-SC Schottky barrier foresees an insulating behavior at a much higher (~100 kHz) frequency (see also below), in the TA sample such a limiting behavior is expected at a lower frequency (around 500 Hz). A possible explanation for such a finding is suggested in the next section.

As for the vacuum-treated sample, the values of differential capacitance changed very much in a large range of frequencies and electrode potential values. Moreover, from the EIS data analysis for such a sample, a behavior almost coincident with that of an ideally polarizable a-SC/El interface, with a negligible contribution coming from surface states, was observed, as described in Ref. 19. According to this, in fitting the DA plots at different frequencies, the electrical equivalent circuit of the junction could be simplified by neglecting the arms in parallel to the arm containing the impedance of a-SC at any investigated frequency for $U_E \geq 0.5$ V/SCE and at any potential for ac frequencies $f \geq 100$ Hz. At the lowest exploited frequencies ($10\ \text{Hz} \leq f \leq 50$ Hz), a very small correction of admittance values was carried out at $U_E \leq 0.5$ V/SCE by using the values of C_{SS} and G_{SS} derived from the EIS data analysis (see Table II).

In Fig. 7, we report for the vacuum-treated sample the inverse of the capacitance a-Nb_2O_5/El junction measured at four different frequencies (10 Hz, 200 Hz, 5 kHz, and 20 kHz). The data plotted in the figure have been corrected for the equivalent series resistance and the Helmholtz double-layer capacitance (20 μF cm^{-2}) as reported in Ref. 19. An evident dependence of the capacitance values from the ac frequency as well as from the electrode potential is observed at variance with all other investigated samples. Both these dependences of the capacitance values agree with the theoretical expectations based on the theory of a-SC Schottky barriers (see below) and at variance with the simplified Mott–Schottky theory of the crystalline SC/El junction. In fact, in this last case, in the absence of the surface-state contribution, frequency-independent capacitance vs potential plots[40-45] are expected as long as a monoenergetic donor distribution is assumed albeit spatially variable.[44,45] The influence of relaxation effects in a very thin surface layer and of deep lying donor distribution in crystalline SC has been taken into account as a possible source of the frequency dependence and nonlinear Mott–Schottky (M-S) plots.[46-48] From the M-S analysis of the curves plotted in Fig. 7 in the low band-bending regime ($U_E - U_{FB} < 0.5$ V), it was possible to get a flatband potential value almost independent of the ac frequency, while the slope of the M-S linear part strongly changed with it. A computer simulation trying to fit the observed behavior by assuming the existence of two donor levels, a shallow one completely ionized and a second one deep lying in the bandgap, failed in fitting the experimental data. These aspects as well as further details on the results of M-S plot simulation will be presented and discussed in a future paper.[49]

Electronic properties and energetics of aged a-Nb_2O_5/El interface.— To get information on the electronic properties of aged niobia and on the location of characteristic energy levels of the a-SC/El junction, we carried out a detailed study of the DA plots in a large range of frequencies (10 Hz–20 kHz). Moreover, owing to an almost ideal blocking behavior of the interface, an electrode potential interval ($U_E - U_{FB} \approx 6$ V) well beyond the onset of the HBB region[16-18,32,33] was exploited.

In all the ranges of exploited frequencies, only the vacuum aged sample displayed an SC-like behavior, while the other samples displayed an insulating-like behavior at any frequency (AF) or at frequency slightly above 50 Hz (AT and TAR).[19] According to this, the DA data of the TV sample are extensively reported in the following. In Fig. 8, we report the experimental data and the fitting curves of the two components of the DA, Y_{SC}, for two frequencies. The fitting of experimental data was carried out by using for the film capacitance and conductance, C_{SC} and G_{SC}, the theoretical expression derived in the hypothesis of a DOS spatially nonhomogeneous but almost constant in energy[18]

$$\frac{1}{C_{SC}(x,\omega,\psi_S)} = \frac{1}{C_{SC}(\omega,\psi_S)} f_\omega[x(\psi_S)] \qquad [6a]$$

$$G_{SC}(x,\omega,\psi_S) = G_{SC}(\omega,\psi_S) g_\omega[x(\psi_S)] \qquad [6b]$$

where $f_\omega[x(y_S)]$ and $g_\omega[x(y_S)]$ are, respectively, two different trial functions depending only on the electrode potential but changing with the employed frequency. The term multiplying the two trial functions can be considered as coincident with the expression of $(C_{SC})^{-1}$ and G_{SC} in the absence of spatial variation in DOS distribution (homogeneous film) but averaged in energy. In the hypothesis of constant DOS and HBB regime, the following analytical expressions for both components of the DA have been derived[18,50]

$$\frac{1}{C_{SC,HBB}(\omega,\psi_S)} = \frac{1}{\sqrt{\varepsilon\varepsilon_0 e^2 N}} \left(\ln\frac{\psi_G}{\psi_C} + \sqrt{1 + \frac{2}{\psi_G}(\psi_S - \psi_G)} \right) \qquad [7a]$$

$$G_{SC,HBB}(\omega,\psi_S) = \pi^2 f \frac{kT}{|e|\psi_C} \sqrt{\varepsilon\varepsilon_0 e^2 N} \times \left(\ln\frac{\psi_g}{\psi_C} + \sqrt{1 + \frac{2}{\psi_G}(\psi_S - \psi_G)} \right)^{-2} \qquad [7b]$$

where N is the DOS in eV^{-1} cm^{-3}, $\psi_S = (U_E - U_{FB})$ is the potential drop within the SC, $\psi_g = (E_g/2 - \Delta E_F)/e$ is the potential at which the Fermi level crosses the half-gap of SC (around 1.35 V in our case), and ψ_C is a characteristic potential in the theory of the a-SC Schottky barrier;[18] the other symbols have their usual meaning. Equations 7a and 7b have been derived under conditions $\psi_S > \psi_C \geq 3k_BT/e$, and they coincide with the low band-bending expression for $\psi_S \leq \psi_G$ [13,18] when the substitution $\psi_G = \psi_S$ is introduced in Eq.

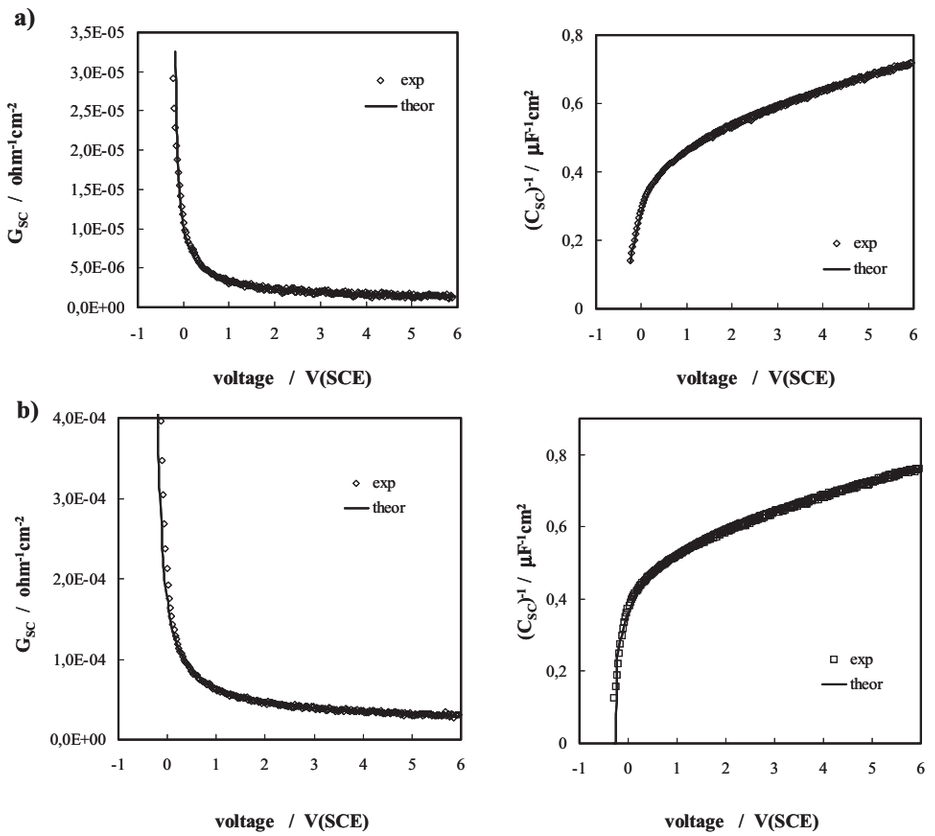

Figure 8. Experimental data and fitting curves of the two components of the DA for the vacuum-treated sample at (a) 10 and (b) 200 Hz according to the theory of a-SC Schottky barrier.

7. As reported in Refs. 32 and 33, the previous equation should be valid also in the presence of a DOS distribution variable with energy, provided that changes in DOS are small within k_BT.

From the theory, it can be shown that ψ_C is given by the relationship

$$|e|\psi_C = |e|\psi(x_C) = -kT\ \ln(\omega\tau_0) - \Delta E_F \qquad [8]$$

where $\Delta E_F = (E_C - E_F)_{bulk}$ represents the distance in energy between the mobility edge, E_C, and the Fermi level, E_F, in the bulk of the a-SC, and $|e|\psi_C$ is the band bending at a distance x_C from the surface of the junction where the cutoff energy level E_ω crosses the Fermi level (as explained in Ref. 18). The cutoff energy level is defined from the conditions

$$\omega\tau = 1 \quad \text{with} \quad \tau = \tau_0\ \exp\left(\frac{E_\omega - E_C}{kT}\right) \qquad [9]$$

where τ is the capture/emission time of electron from the localized energy level E to/from the conduction band mobility edge $E_{C,m}$. It comes out that x_C changes with changing frequency, ω, and band bending ψ_S. In particular, x_C increases with increasing frequency at constant polarization or with increasing polarization at constant frequency. It is the dependence of x_C from the ac frequency that is reflected mainly in the frequency dependence observed in the a-SC/El junction. More details on these aspects can be found in Ref. 16-18 and 31-35.

At variance with the usual M-S approach, the flatband potential is now derived as a common fitting parameter of the two components of admittance curves, G_{SC} and C_{SC} vs U_E plots, at various frequencies with the constraint on ψ_C

$$d\psi_C/d\ \log\ f = -2.3kT/|e| = -59\ \text{mV/decade} \qquad [10]$$

To reduce the arbitrariness of the ψ_C value to be used in the fitting procedure, we recall that, according to Eq. 7, the zeroing of the ψ_C value should occur at a frequency where a constant capacitance value is measured for any $U_E \geq (U_{FB} + 3k_BT/e)$. In fact, at such a frequency x_C should reach the metal/oxide interface, and the entire film behaves like a dielectric of constant thickness ($C_{SC} = \varepsilon_{ox}\varepsilon_0/d_{ox}$). In Table III, we report the flatband potential values derived from fitting at all investigated frequencies from which an average U_{FB} value of -0.42 ± 0.025 V/SCE was estimated for the TV niobia/H_2SO_4 solution interface. The fitting of experimental curves was carried out by accepting a difference in the U_{FB} values for the two components of the admittance in the order of k_BT/e volt. The use of a variable dielectric constant does not appreciably change the fitting parameter reported in Table III owing to the small change in electric field values estimated by assuming the thickness of the semiconducting oxide equal to the total measured oxide thickness (157–159 nm).

The flatband potential value for TV anodic niobia appears much more ($\sim$0.2 V) cathodic than the value reported for thin and thick

Table III. Parameters obtained from the analysis of the DA curves at different frequencies for the TV sample.

f (Hz)	ψ_C (mV)	U_{FB} from C_{SC} [V(SCE)]	U_{FB} from G_{SC} [V(SCE)]
10	230	−0.432	−0.427
20	210	−0.427	−0.412
50	188	−0.422	−0.402
100	171	−0.432	−0.412
200	152	−0.436	−0.415
500	130	−0.417	−0.417
1000	112	−0.432	−0.422
2000	92	−0.427	−0.417
5000	70	−0.437	−0.417
10000	53	−0.437	−0.417

untreated anodic oxides. By taking into account that no appreciable change in the optical bandgap (tailing included) was evidenced by PCS data, we conclude that the cathodic shift in the U_{FB} value of the TV sample, with respect to the as-formed one, agrees with the hypothesis of an increased concentration of donor species due to an increase in the Nb/O ratio. The U_{FB} value agrees reasonably well with the V^* value derived from PCS measurements within the experimental uncertainty. As for the location of characteristic energy levels (E_F and E_C), we make use of the relationships

$$E_F^0(\mathrm{El}) = eU_{FB} \quad [11]$$

$$E_{C,bulk} = E_{F,bulk} - kT\ \ln(\omega\tau_0) - |e|\psi_C(\omega) \quad [12]$$

In the absence of further information, we can locate the mobility band conduction edge of n-type a-SC, once a value of ψ_C at any arbitrary frequency is known, by using for τ_0 an average value of 10^{-12} s. By using for ψ_C the value (0.23 V) reported in Table III for $f = 10$ Hz, we can locate the conduction band mobility edge, $E_{C,m}$, 0.37 eV above E_F. The conduction band mobility edge, $E_{C,m}$, calculated according to the theory of the a-SC Schottky barrier, stays about 0.35 eV higher in energy than the conduction bandedge estimated by using the approach based on the traditional M-S model for crystalline SC.[49] The location of the valence band mobility edge $E_{V,m}$ can be carried out by using the optical bandgap reported above (3.45 eV).

As for the differential capacitance behavior of TA and TAR samples at various frequencies, although in agreement with the amorphous nature of the oxides as evidenced above, a big difference can be traced out to the measured value of the differential capacitance of the junction at the highest (20 kHz) employed frequency (see Fig. 6). After re-anodizing, the differential capacitance behavior of the air-treated sample, as a function of the frequency, appears in agreement with the fact that a more stoichiometric (insulating) oxide is formed, so that the Fermi level of the a-SC decreases below the cutoff energy level E_ω at a relatively low ac frequency. However, in TA and TAR samples a frequency window ($10 \leq f \leq 50$ Hz), centered at around 20 Hz, was found, in which the constraint ($\psi_C \geq 0.075$ eV) underlying the validity of Eq. 7 holds. According to this, we report for both samples in Fig. 9a and b the best fit of DA results at 10 Hz, from which the flatband potential and DOS distribution as a function of the distance from the oxide/El interface could be derived. To make an easy comparison with the TV sample, the same equivalent circuit (absence of any C_{SS} contribution) was used to fit the differential capacitance data.

Analogously to the V^* data in Table I, very different U_{FB} values were derived for the two samples with the most cathodic one (−0.41 V/SCE) pertaining to the TA sample, while the TAR sample displayed a much more anodic U_{FB} value (~−0.14 V/SCE). As mentioned before in the TAR sample, the measured value of capacitance (at 10 Hz) was very close to the value expected if all the films behave like a dielectric. The shift in U_{FB} toward the anodic direction, as well as the value derived from the DA measurements, agrees with the more insulating behavior of the TAR sample with respect to the TA sample and with the PCS data reported in Table I.

In the TA film, the capacitance at 10 Hz is not too far from the value measured at 20 kHz, and, also at this frequency, the measured capacitance accounts for a space-charge region length much less than the total film thickness. An estimate of the thickness of the TA sample behaving as a dielectric layer can be carried out by using the capacitance value measured at 20 kHz, together with the values of the dielectric constant reported above, 53–56. From such a calculation, a dielectric film thickness equal to about 65–70% of the total thickness (159 nm) is estimated, thus suggesting that some metallization of the inner oxide layer occurs, although the largest external part of the film still behaves as an insulating-like a-SC. The flatband potential (−0,41 V/SCE) obtained from best-fitting of the differential capacitance plot of the TA sample is slightly more negative than V^* (see Table I) and quite near to that derived for the TV sample.

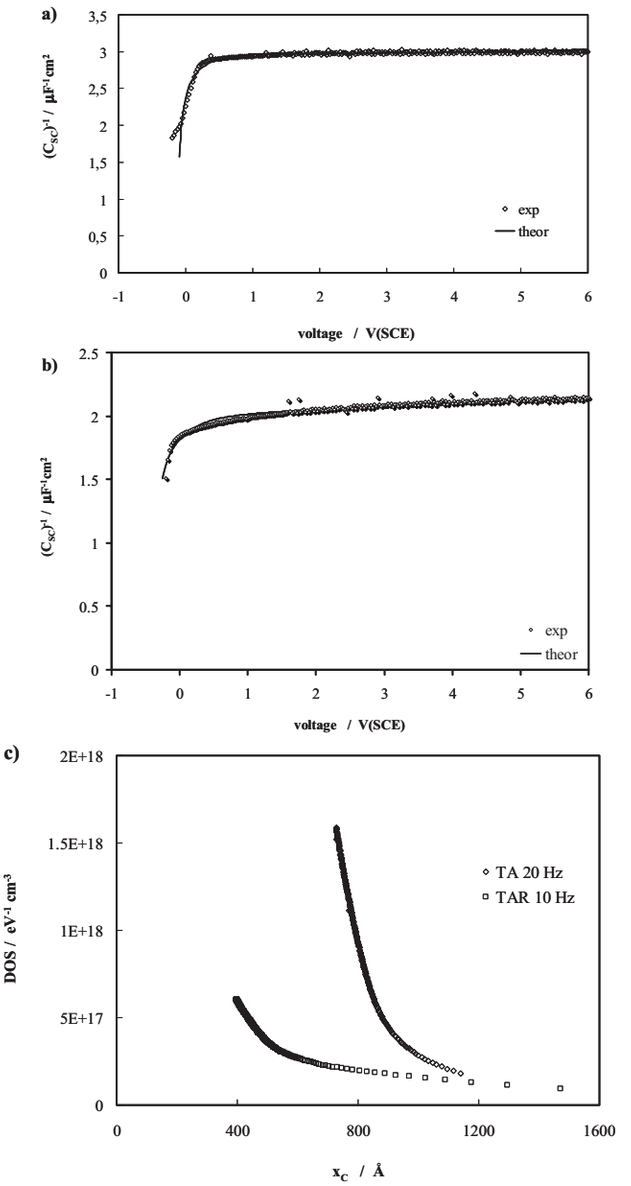

Figure 9. Experimental data and fitting curves of the inverse of the differential capacitance at 10 Hz. (a) TAR sample: $e\psi_c = 0.075$ eV, $U_{FB} = -0.17$ V/SCE; (b) TA sample: $e\psi_c = 0.095$ eV, $U_{FB} = -0.41$ V/SCE. (c) DOS distribution as a function of x_C for TAR and TA samples.

DOS distribution as a function of metal/oxide distance and energy distance from E_F.— By taking advantage of the spectroscopic character[31-34] of the $G_{SC}(\omega)$ vs U_E plots, it is possible to get further information on the DOS distribution as a function of the distance from the metal/oxide interface as well as from the Fermi level distance. In fact, from $G_{SC}(\omega)$ vs U_E plots, at different frequencies, it is possible to derive the spatial variation in DOS at the corresponding energy level, $E_F - |e|\psi_C(\omega)$, as

$$N(E_F - |e|\psi_C) = \frac{2}{\pi kT}\frac{G_{SC}(\psi_{SC},\omega)/\omega}{C_{SC}^2(\psi_{SC},\omega)} f_\omega[x(\psi_{SC})]C(\psi_C,0) \times \int_{E_F-|e|\psi_C}^{E_F} N(E)dE \quad [13]$$

and by substituting to the integral the term $|e|\psi_C N_{av}$. As a first ap-

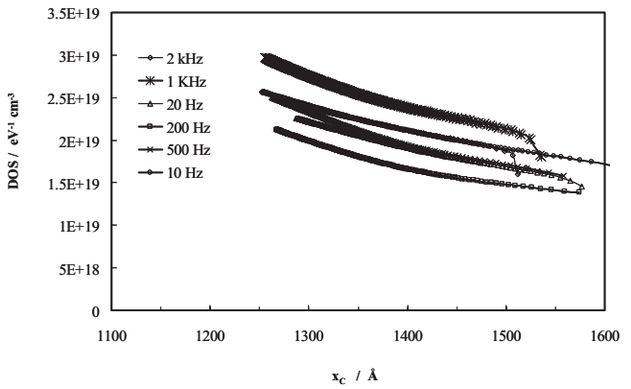

Figure 10. Plots of DOS distribution as a function of x_C at different frequencies for TV sample.

proximation for N_{av}, that one derived from the fitting of C_{SC} at the same ω and x_C values has been chosen. At constant x_C (i.e., at a fixed distance from the oxide/El interface), but variable frequency, the DOS distribution at a distance $|e|\psi_C$ in energy below E_F is obtained.[18]

As for the TA and TAR samples, we report in Fig. 9c the DOS distribution as a function of the distance from the metal/oxide interface, from which it comes out that for both samples at equal distance from the oxide/El interface, the DOS distribution ($\sim 10^{17}$ eV^{-1} cm^{-3}) is about 2 orders of magnitude lower than that reported ($\sim 10^{19}$ eV^{-1} cm^{-3}) for the TV sample (see Fig. 10). These results could help to explain the disappearance of tailing in the photocurrent spectra of the TA and TAR samples as mentioned above. In fact, according to the theory of optical transitions in amorphous materials,[21,25] a much lower intensity of photocurrent (lower optical absorption coefficient) can be expected for these samples at photon energies below the mobility gap where the DOS is about 2 orders of magnitude lower than that in the TV sample. The disappearance of the tails in photocurrent spectra as well the large decrease in DOS evidenced from DA measurements are a strong support in favor of a rapid (exponential-like) decrease in localized states near the two mobility edges.

In Fig. 10, we report the DOS distribution as a function of x_C at different frequencies for the TV sample. The dependence of the DOS from the solution/oxide interface distance, at any frequency, suggests a spatially increasing concentration of DOS on going from the oxide/El interface [$N_{av} \approx (1.9 \pm 0.3) \times 10^{19}$ cm^{-3} eV^{-1}] toward the metal/oxide interface, with an average value of DOS at about 30 nm from the oxide/El interface equal to $N_{av} \approx (2.5 \pm 0.4) \times 10^{19}$ cm^{-3} eV^{-1}. By interpolating the data of Fig. 10 by using a second-order polynomial law, N_{av} values on the order of $\sim(1–3) \times 10^{20}$ cm^{-3} eV^{-1} are obtained for the DOS value at the metal/oxide interface. Such values are not unrealistic although almost 1 (or 2) order of magnitude higher than that derived for the TA (or TAR and AF) sample. However, for these last samples the DOS estimates are very approximate owing to the very limited range of exploited frequencies.

An estimate of the DOS distribution, at an energy $|e|\psi_C(\omega)$ below E_F, can be obtained from Fig. 10 at a fixed distance from the oxide/solution interface for different values of x_C spanning a region of the film wide about 20% of total film thickness (distance from El/film interface ranging from ~5 to ~30 nm). From such plots, it comes out that in an energy window of ~0,14 eV (10 Hz–2 kHz), an almost energy-independent electronic DOS distribution is derived for the TV sample. At higher frequencies (i.e., for energy levels nearer to E_F), the DOS distribution increases as theoretically assumed for fitting the EIS spectra.[19]

The dependence of DOS on the metal/oxide distance has been evidenced in previous works on Nb anodic films, not subjected to any thermal treatment, and it seems a quite general trend for anodic films on valve metals.[14,36] However, according to the literature data,[3,13,14] in the presence of thermal aging under vacuum, the possibility of a larger decrease in the oxygen/metal ratio in the inner part of the oxide must be taken into account owing to the tendency of oxygen to diffuse into Nb metal. According to this, the formation of substoichiometric $Nb_2O_{(5-x)}$,[1,3,24,51] having possibly metallic properties,[52] in the inner part of the anodic oxide cannot be ruled out for both TV and TA samples. This suggestion should agree with the DA measurements if we consider that a good fitting of DA results was obtained by assuming a true semiconducting behavior for the most exterior part of the oxide having a thickness in the range of ~50 nm for the TV sample and ~100 nm for the TA sample. A fitting of the DA curves in such a hypothesis was also carried out, showing that with respect to the previous results, only very minor changes in the U_{FB} or ψ_C values were necessary, while appreciable differences appeared in the DOS distribution. Further experiments are now in progress trying to determine the spatial extent of changes in oxygen/metal ratio in the inner oxide regions.

Conclusions

From the detailed investigation based on PCS, EIS, and DA measurements in a rather large range of frequencies and electrode potentials, a quite self-consistent picture of the solid-state and electronic properties of as-formed and thermally treated anodic niobia appears. A unifying approach based on the theory of amorphous SC is able to rationalize the photoelectrochemical and electrical behaviors of untreated and thermally aged amorphous niobia films. The use of magnetron-sputtered niobium film allowed us to minimize the interference of the surface treatment usually reflected in the spurious frequency dependence of the circuital elements introduced in fitting EIS data.

In this work, the behavior of anodic niobia films after thermal treatment under vacuum (TV) can be interpreted in agreement with the behavior expected for the a-SC junction barrier behaving as an ideally polarizable interface. According to the theory, an almost constant flatband potential of $U_{FB} = -0.42 \pm 0.025$ V/SCE has been derived for the vacuum-treated sample in 0.5 M H_2SO_4 solution in a large range of exploited ac frequencies. Such a value is more cathodic than that of the as-formed anodic film owing to a shift in the Fermi level of the oxide toward the conduction band mobility edge. This shift, observed only for thermally treated electrodes, is attributed to the decrease in the oxygen/metal ratio due to the oxygen diffusion inside the metallic substrate with a consequent filling of the vacant localized state lying within the mobility gap of the amorphous semiconducting niobia.

Both the thermal treatment and the re-anodizing process affect the solid-state properties of the as-formed and vacuum-treated samples in a different way, as evidenced by the PCS study. Subtle changes in the DOS distribution occurs as a consequence of the different treatments, and such changes have been evidenced by both photoelectrochemical and DA studies.

Acknowledgments

This work has been partially supported by Palermo University (ex-60% Funds).

References

1. H. Habazaki, M. Yamasaki, T. Ogasawara, K. Fushimi, H. Konno, K. Shimizu, T. Izumi, R. Matsuoka, P. Skeldon, and G. E. Thompson, *Thin Solid Films*, **516**, 991 (2008).
2. L. Young, *Anodic Oxide Films*, Academic, London (1961).
3. K. Kovacs, G. Kiss, M. Stenzel, and H. Zillgen, *J. Electrochem. Soc.*, **150**, B361 (2003).
4. Y. Matsui, M. Hiratani, S. Kimura, and I. Asano, *J. Electrochem. Soc.*, **152**, F54 (2005).
5. S. Semboshi, K. Bando, N. Ohtsu, Y. Shim, and T. J. Konno, *Thin Solid Films*, **516**, 8613 (2008).
6. H. Habazaki, T. Matsuo, H. Konno, K. Shimizu, K. Matsumoto, K. Takayama, Y. Oda, P. Skeldon, and G. E. Thompson, *Surf. Interface Anal.*, **35**, 618 (2003).
7. S. Ono, K. Kuramochi, and H. Asoh, *Corros. Sci.*, **51**, 1513 (2009).
8. C. S. Kim, S. J. Jo, S. W. Lee, W. J. Kim, H. K. Baik, and S. J. Lee, *J. Electrochem.*

Soc., **154**, H102 (2007).
9. G. M. Wang, D. Moses, A. J. Heeger, H. M. Zhang, M. Narasimhan, and R. E. Demaray, *J. Appl. Phys.*, **95**, 316 (2004).
10. M. Erouel, A. Gagnaire, A. L. Deman, J. Tardy, N. Jaffrezic-Renault, Z. Sassi, J. C. Bureau, and M. A. Maaref, in *Passivation of Metals and Semiconductors, and Properties of Thin Oxide Layers*, P. Marcus and V. Maurice, Editors, p. 271, Elsevier, Paris (2006).
11. F. Di Quarto, V. Figà, P. Bocchetta, and M. Santamaria, *Electrochem. Solid-State Lett.*, **10**, H305 (2007).
12. H. Habazaki, T. Ogasawara, H. Konno, K. Shimizu, K. Asami, K. Saito, S. Nagata, P. Skeldon, and G. E. Thompson, *Electrochim. Acta*, **50**, 5334 (2005).
13. F. Di Quarto, C. Sunseri, and S. Piazza, *Ber. Bunsenges. Phys. Chem.*, **90**, 549 (1986).
14. F. Di Quarto, S. Piazza, and C. Sunseri, *Electrochim. Acta*, **35**, 99 (1990).
15. A. G. Munoz and G. Staikov, *J. Solid State Electrochem.*, **10**, 329 (2006).
16. F. Di Quarto, F. La Mantia, and M. Santamaria, in *Passivation of Metals and Semiconductors, and Properties of Thin Oxide Layers*, P. Marcus and V. Maurice, pp. 343–348, Elsevier, Paris (2006).
17. F. Di Quarto, F. La Mantia, and M. Santamaria, *Corros. Sci.*, **49**, 186 (2007).
18. F. Di Quarto, F. La Mantia, and M. Santamaria, *Electrochim. Acta*, **50**, 5090 (2005).
19. F. La Mantia, M. Santamaria, H. Habazaki, and F. Di Quarto, *ECS Trans.*, **19**(3), 411 (2009).
20. F. Di Quarto, C. Sunseri, S. Piazza, and M. Santamaria, in *Handbook of Thin Films*, Vol. 2, H. S. Nalwa, p. 373, Academic, San Diego (2002).
21. F. N. Mott and E. A. Davis, *Electronic Processes in Non-Crystalline Materials*, 2nd ed., Clarendon, Oxford (1979).
22. M. A. Butler, *J. Appl. Phys.*, **48**, 1914 (1977).
23. F. Di Quarto, S. Piazza, R. D'Agostino, and C. Sunseri, *J. Electroanal. Chem.*, **228**, 119 (1987).
24. H. Oechsner, J. Giber, H. J. Fusser, and A. Darlinski, *Thin Solid Films*, **124**, 199 (1985).
25. W. E. Spear, H. Al-Ani, and P. G. Le Comber, *Philos. Mag. B*, **43**, 781 (1981).
26. P. Agarwal, M. E. Orazem, and L. H. GarciaRubio, *J. Electrochem. Soc.*, **142**, 4159 (1995).
27. F. La Mantia, J. Vetter, and P. Novak, *Electrochim. Acta*, **53**, 4109 (2008).
28. C. D. Jaeger, H. Gerischer, and W. Kautek, *Ber. Bunsenges. Phys. Chem.*, **86**, 20 (1982).
29. G. Oskam, D. Vanmakaelbergh, and J. J. Kelly, *Electrochim. Acta*, **38**, 301 (1993).
30. W. P. Gomes and D. Vanmakaelbergh, *Electrochim. Acta*, **41**, 967 (1996).
31. R. A. Abram and P. J. Doherty, *Philos. Mag. B*, **45**, 167 (1982).
32. J. D. Cohen and D. V. Lang, *Phys. Rev. B*, **25**, 5321 (1982).
33. D. V. Lang, J. D. Cohen, and J. P. Harbison, *Phys. Rev. B*, **25**, 5285 (1982).
34. I. W. Archibald and R. A. Abram, *Philos. Mag. B*, **48**, 111 (1983).
35. I. W. Archibald and R. A. Abram, *Philos. Mag. B*, **54**, 421 (1986).
36. F. Di Quarto, V. O. Aimiuwu, S. Piazza, and C. Sunseri, *Electrochim. Acta*, **36**, 1817 (1991).
37. H. Habazaki, T. Ogasawara, H. Konno, K. Shimizu, S. Nagata, K. Asami, K. Takayama, P. Skeldon, and G. E. Thompson, *J. Electrochem. Soc.*, **153**, B173 (2006).
38. Y. M. Li and L. Young, *J. Electrochem. Soc.*, **147**, 1344 (2000).
39. J. L. Ord, W. P. Wang, and M. A. Hopper, *J. Electrochem. Soc.*, **119**, 439 (1972).
40. H. O. Finklea, *J. Electrochem. Soc.*, **129**, 2003 (1982).
41. J. F. Dewald, *Bell Syst. Tech. J.*, **39**, 615 (1960).
42. J. F. Dewald, *J. Phys. Chem. Solids*, **14**, 155 (1960).
43. A. Hamnett, in *Comprehensive Chemical Kinetics*, Vol. 27, R. G. Compton, Editor, p. 100, Elsevier Science, Oxford (1987).
44. M. H. Dean and U. Stimming, *J. Electroanal. Chem.*, **228**, 135 (1987).
45. M. H. Dean and U. Stimming, *J. Phys. Chem.*, **93**, 8053 (1989).
46. E. C. Dutoit, R. L. Van Meirhaeghe, F. Cardon, and W. P. Gomes, *Ber. Bunsenges. Phys. Chem.*, **79**, 1206 (1975).
47. G. Nogami, *J. Electrochem. Soc.*, **133**, 525 (1986).
48. D. B. Bonham and M. E. Orazem, *AIChE J.*, **34**, 465 (1988).
49. F. La Mantia, H. Habazaki, M. Santamaria and F. Di Quarto, *Russ. J. Electrochem.*, Accepted for publication.
50. C. da Fonseca, M. G. Ferreira, and M. da Cunha Belo, *Electrochim. Acta*, **39**, 2197 (1994).
51. Q. Ma and R. A. Rosenberg, *Appl. Surf. Sci.*, **206**, 209 (2003).
52. L. Nagarajan, R. A. De Souza, D. Samuelis, I. Valov, A. Borger, J. Janek, K. D. Becker, P. C. Schmidt, and M. Martin, *Nat. Mater.*, **7**, 391 (2008).